NANO LETTERS

Letter

pubs.acs.org/NanoLett

Ultrafast Dynamics of Lasing Semiconductor Nanowires

Robert Röder,*[,†] Themistoklis P. H. Sidiropoulos,[‡] Christian Tessarek,[§,∥] Silke Christiansen,[§,∥] Rupert F. Oulton,[‡] and Carsten Ronning*[,†]

[†]Institute of Solid State Physics, Friedrich-Schiller-University Jena, Max-Wien-Platz 1, 07743 Jena, Germany

[‡]Imperial College London, Prince Consort Road, SW7 2BZ London, United Kingdom

[§]Max Planck Institute for the Science of Light, Günther-Scharowsky-Strasse 1, 91058 Erlangen, Germany

[∥]Helmholtz Center Berlin for Materials and Energy, Hahn-Meitner-Platz 1, 14109 Berlin, Germany

Supporting Information

ABSTRACT: Semiconductor nanowire lasers operate at ultrafast timescales; here we report their temporal dynamics, including laser onset time and pulse width, using a double-pump approach. Wide bandgap gallium nitride (GaN), zinc oxide (ZnO), and cadmium sulfide (CdS) nanowires reveal laser onset times of a few picoseconds, driven by carrier thermalization within the optically excited semiconductor. Strong carrier−phonon coupling in ZnO leads to the fastest laser onset time of ∼1 ps in comparison to CdS and GaN exhibiting values of ∼2.5 and ∼3.5 ps, respectively. These values are constant between nanowires of different sizes implying independence from any optical influences. However, we demonstrate that the lasing onset times vary with excitation wavelength relative to the semiconductor band gap. Meanwhile, the laser pulse widths are dependent on the optical system. While the fastest ultrashort pulses are attained using the thinnest possible nanowires, a sudden change in pulse width from ∼5 to ∼15 ps occurs at a critical nanowire diameter. We attribute this to the transition from single to multimode waveguiding, as it is accompanied by a change in laser polarization.

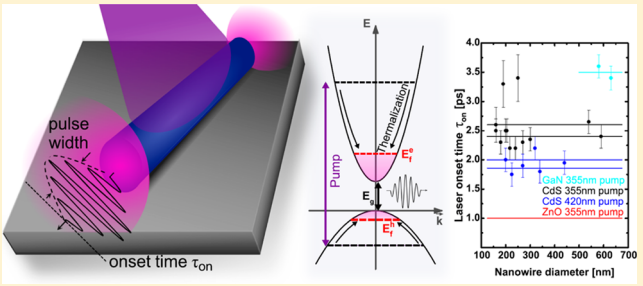

KEYWORDS: *Semiconductor nanowire, ultrafast lasing, onset time, pulse width, carrier thermalization, carrier−phonon interaction*

The immense progress in understanding the properties of semiconductor nanowire (NW) lasers has led to ideas that exploit coherent radiation available at dimensions below the wavelength barrier.[1,2] Besides promising concepts in single molecule sensing,[3−5] nonlinear frequency generation,[6,7] and optical switching,[8] the recent development of nanophotonics and photonic circuitry requires NW lasers as nanoscale light sources to overcome the drawbacks of conventional electronic circuitry. A semiconductor NW, made from a high optical gain material,[9,10] intrinsically provides efficient waveguiding[11] as well as resonator feedback at the end facets; thus, single NWs form the smallest laser oscillators based on photonic modes[12,13] suited to fulfill these requirements. Indeed, optically pumped semiconductor NW lasers operating at room temperature and even in continuous emission mode[14] now consequently occupy the spectrum from the UV to the NIR;[15−18] also, fundamental polarization features[19,20] and resonator modification treatments have been demonstrated.[21,22] While the fundamentals of NW lasers like emission wavelength, polarization properties, and cavity modification have been studied thoroughly, the temporal dynamics of these lasers remain relatively unstudied, mainly due to their ultrafast response times, which are difficult to measure. Meanwhile, knowledge of NW laser operation speed is crucial to assess the potential of these devices as coherent nanoscale light sources in real world applications. The laser dynamics include the onset time of the nanolaser, which is mainly determined by carrier thermalization in the semiconductor as well as the gain recovery time and the output pulse width, which are influenced by optical geometry and cavity modes.

In this study, we used a double-pump approach exploiting the nonlinearity of the NW laser process itself to access the ultrafast laser dynamics[23] and studied them thoroughly for different material systems. We first studied the dynamics of cadmium sulfide (CdS) NW lasers in detail and show a route to tune the laser onset time without influencing the remaining laser features. Subsequently, we demonstrate the respective dynamics for gallium nitride (GaN) NW lasers. By comparing both results to data from zinc oxide (ZnO) NW lasers,[23] we gain insight into the fundamental material properties that determine the laser onset time, which is completely independent of the emission wavelength. Additionally, we determined the output pulse width for all material systems investigated.

Both, CdS NWs as well as GaN NWs were synthesized using the vapor−liquid−solid (VLS) mechanism. A thermal transport

Received: April 8, 2015
Revised: June 4, 2015
Published: June 18, 2015

DOI: 10.1021/acs.nanolett.5b01271
Nano Lett. 2015, 15, 4637−4643

technique of atomic species was exploited for the growth of CdS NW batches in a horizontal tube furnace according to the growth parameters given in ref 17, while the GaN NWs were grown in a metal−organic vapor phase epitaxy (MOVPE) reactor as described in ref 24. The bare NWs were transferred onto a low refractive index SiO_2/Si substrate (1.5 μm thermally grown SiO_2 layer with a refractive index $n \sim 1.4$ on top of Si) in order to avoid the leakage of the electromagnetic field into the substrate and thus ensuring a photonic mode largely confined within the NW optical cavity.[14] The Fabry-Pérot (FP) like cavity is defined by the NW length (5 μm < L < 30 μm) in which the confined transverse mode propagates back and forth along the NW axis exhibiting an effective reflectivity at the end-facets with values of ∼50%[25] (in CdS with values up to ∼56%[20]). The utilized semiconductor materials are furthermore capable of providing strong optical gain with values higher than 10^3 cm^{-1} to induce lasing in a single NW.[13,17,9] Under strong optical excitation, carrier densities exceeding the Mott density result in the formation of an electron−hole plasma (EHP) with sufficiently high gain to be accompanied by bandgap renormalization. Thus, the NW lasing spectrum is energetically located slightly below the bandgap of the semiconductor.[10]

Initially, the lasing performance of our NW lasers was thoroughly checked by a power-dependent measurement and the accompanied emission spectra showed the expected discrete laser modes evolving with increasing pump power. Subsequently, the double-pump technique was applied to unravel their ultrafast dynamics,[23] as it is schematically shown in Figure 1a. For the lasing as well as for the double-pump measurements, the single NWs were optically excited at a wavelength of 355 nm. To highlight the pump energy-dependent carrier relaxation time, some NWs were excited with a 420 nm pump wavelength. The wavelength tunable excitation source delivers nominally 150 fs pulses at an adjustable repetition rate, chosen between 266 and 800 kHz to avoid damage or modification of the devices' responses by heating. Figure 1b,c displays the expected response of the NW laser system to the double-pump excitation according to ref 23, where a more detailed description of the technique can be found. In this study, we only refer to time delays of $\tau > 0$: the first strong pulse "Pump1" is sufficient to induce lasing, as it inverts the laser levels to $\Delta N/N_T > 0$, where ΔN depicts the difference between population in the upper and the lower laser level and N_T is the total number of excited carriers. By generating the output pulse at time t_1, the inverted population state gets successively depleted. The weaker pulse "Pump2" approaching at a time delay τ is not able to induce lasing on its own and effectively samples the laser process. For example, if Pump2 arrives after Pump1, it may significantly affect the laser's response by adding newly excited carriers to an already excited carrier population near threshold. A simple semiconductor laser model captures the salient features of the laser's output power, which is obtained by integrating the cavity photon number s/s_{max}, as a function of the time delay. Two clearly distinguishable situations are illustrated in Figure 1c. At short time delays τ, when the inversion remains still close to its peak value, the Pump2 adds excited carriers to the already excited population resulting in an amplification of the first output pulse. The strong pulse, furthermore, causes a significantly reduced material absorption of the second pulse due the built up inversion (Figure 1c). At slightly longer time scales, increasing absorption of Pump2 leads to a second output pulse at a time τ_m after the first output pulse. The output of the double-pump

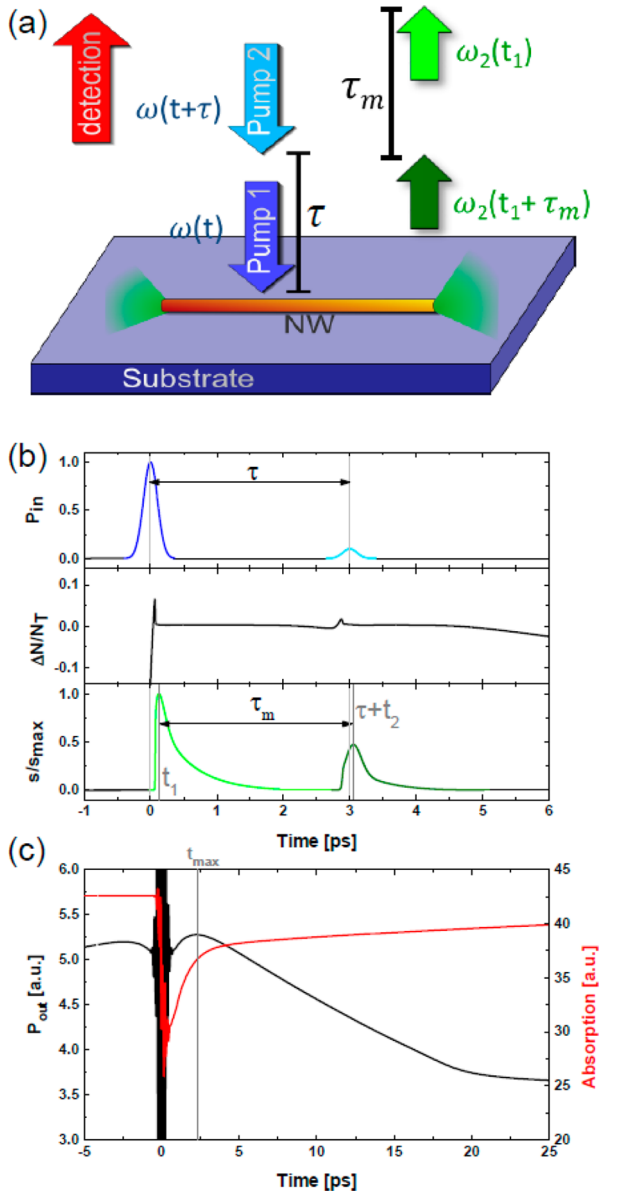

Figure 1. (a) Schematic drawing of the measurement geometry in the double-pump technique and the emission of a semiconductor nanowire (NW) laser lying on a low refractive index substrate (SiO_2). The nanolaser is optically pumped with two pump pulses, which are time-delayed by τ. The first output pulse is emitted at the time t_1 after the first pump pulse (Pump1) has arrived, while the second output pulse is delayed by τ_m relative to the first output pulse. (b) The three graphs show the response of the strong (Pump1) and the weak (Pump2) pump pulses with power (P_{in}), the difference in population ΔN between excited (upper laser) level and ground (lower laser) level normalized to maximum inversion N_T, and the normalized cavity photon number s/s_{max} for a NW laser. (c) Simulation of the output response P_{out} (black, left axis) to the two pump pulses. The output power P_{out} reflects the integration of the cavity photon number from (b) at each time delay. The excitation density was set to twice the threshold value according the experimental conditions. The simulated absorption response (red, right axis) during the double-pump experiment shows the material's gain depletion and recovery during the laser pulse. The simulations are adopted from ref 23.

measurement reaches the maximum at t_{max} exactly when the absorption of the second pulse recovers. This time therefore determines the termination of the first output pulse. At large

DOI: 10.1021/acs.nanolett.5b01271
Nano Lett. 2015, 15, 4637−4643

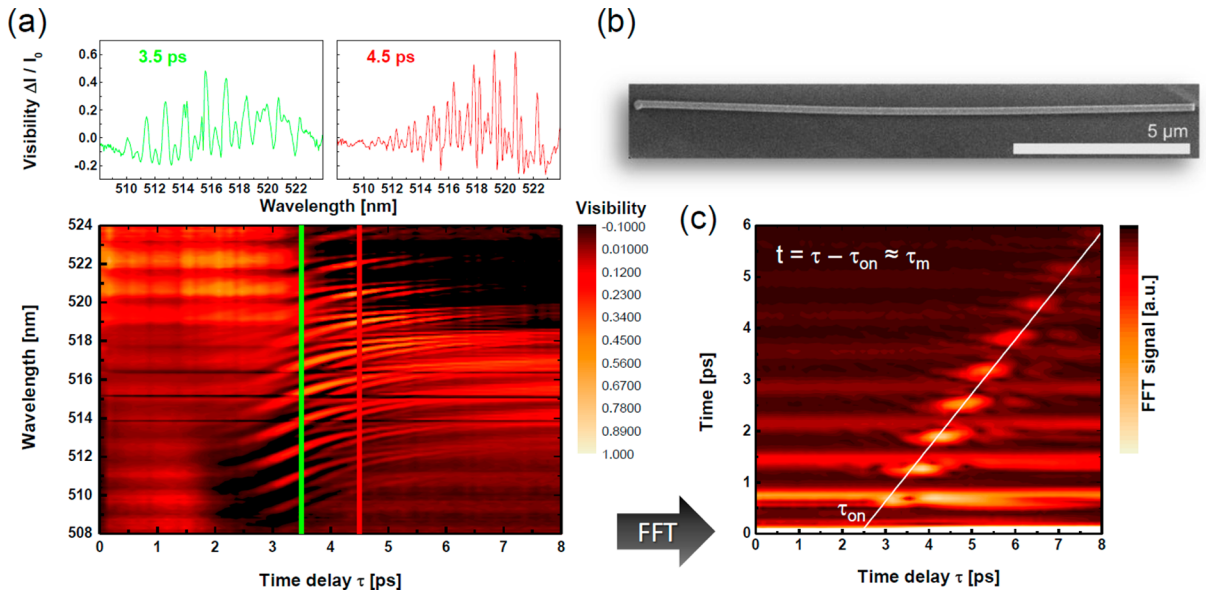

Figure 2. (a) Visibiliy plot (normalized difference spectrum) $\Delta I(\lambda,\tau)/I_0(\lambda) = I(\lambda,\tau)/I_0(\lambda) - 1$ of the CdS nanowire laser (length 15.9 μm, diameter ≈190 nm), which is shown in the SEM image of (b). Here $I(\lambda,\tau)$ is the microphotoluminescence (μPL) spectrum at double-pump excitation and $I_0(\lambda)$ is the μPL spectrum at single strong pulse pumping. The strong [weak] Pump1 [Pump2] was set to twice [0.2 times] the lasing threshold. The left [right] upper panel shows the visibility $\Delta I(\lambda,\tau)/I_0(\lambda)$ spectrum for the time delay τ = 3.5 ps [4.5 ps] as marked in the lower visibility plot by vertical colored lines indicating the increasing spectral modulation frequency with pulse delay. The pumping wavelength was set to 355 nm. (c) Fourier transform of each spectrum of the lower color plot in (a) as a function of time delay τ. The white line indicates the trend $t = \tau - \tau_{on} \approx \tau_m$. The x-axis intersect of this trend indicates τ_{on} = 2.5 ps.

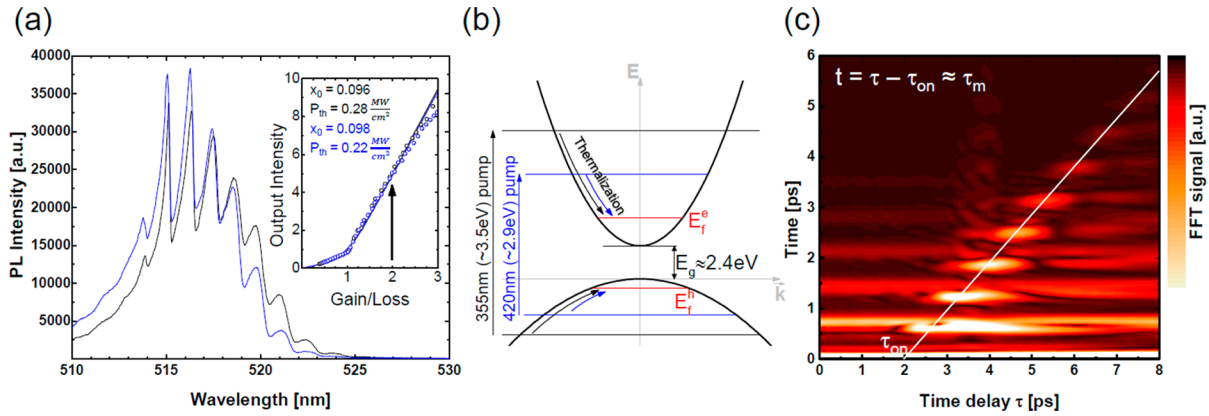

Figure 3. (a) Lasing μPL spectra of the CdS NW shown in Figure 2b at pumping wavelengths of 355 nm (black) and 420 nm (blue) unambiguously show Fabry-Pérot lasing modes dominating the signal at an excitation of twice the threshold P_{th} as marked by the arrow in the power dependence (inset). The emitted output power versus the gain/loss ratio in the inset clearly shows the coincidence of the laser characteristic (with different lasing thresholds P_{th}) for both pumping wavelengths with a value $x_0 \approx 0.1$ as obtained by the model fits using ref 26, that are shown as line. (b) Schematic band diagram of CdS with parabolic conduction and valence bands clarifies the situation for changing the pumping wavelength from 355 to 420 nm. The distribution of excited charge carriers (horizontal lines) therefore gets closer to the respective quasi Fermi levels (E_f^e, E_f^h) of the electron hole plasma causing a decreased relaxation time. (c) The Fourier transform of the double-pump measurement that was obtained similar to Figure 2c for the same CdS NW but at 420 nm pumping with τ_{on} = 2.0 ps.

time delays $\tau > t_{max}$, both output pulses cannot interact anymore and the second pulse just probes the spontaneous decay of the residual excited population.

As we will show later, the predictions made by this simple model fit the experimental observations and enable us to determine the termination time of the NW laser output pulse relatively to the optical pump (t_{max}). However, to gain further insights, especially into the laser onset time τ_{on}, we need to measure the NW laser output temporally as well as spectrally. Figure 2 illustrates the respective results for the CdS NW, shown in 2b, excited with the strong and the weak pump set to powers approximately twice and 0.2 times the laser threshold, respectively. Note that this relative values for Pump1 and Pump2 are applied to all NW lasers during the double-pump measurement. However, for this particular CdS NW the threshold, strong, and weak pump powers are ~0.28, 0.53, and 0.06 MW/cm^2, respectively. As illustrated in Figure 1b, the NW emits two output pulses separated by τ_m with an interference that causes a modulation of the spectral intensity measurable in the spectrometer

$$\Delta I(\omega;\tau) = 2E_1(\omega;\tau)E_2(\omega;\tau)\cos(\omega\tau_m + \Delta\phi(\omega;\tau)) \quad (1)$$

DOI: 10.1021/acs.nanolett.5b01271
Nano Lett. 2015, 15, 4637−4643

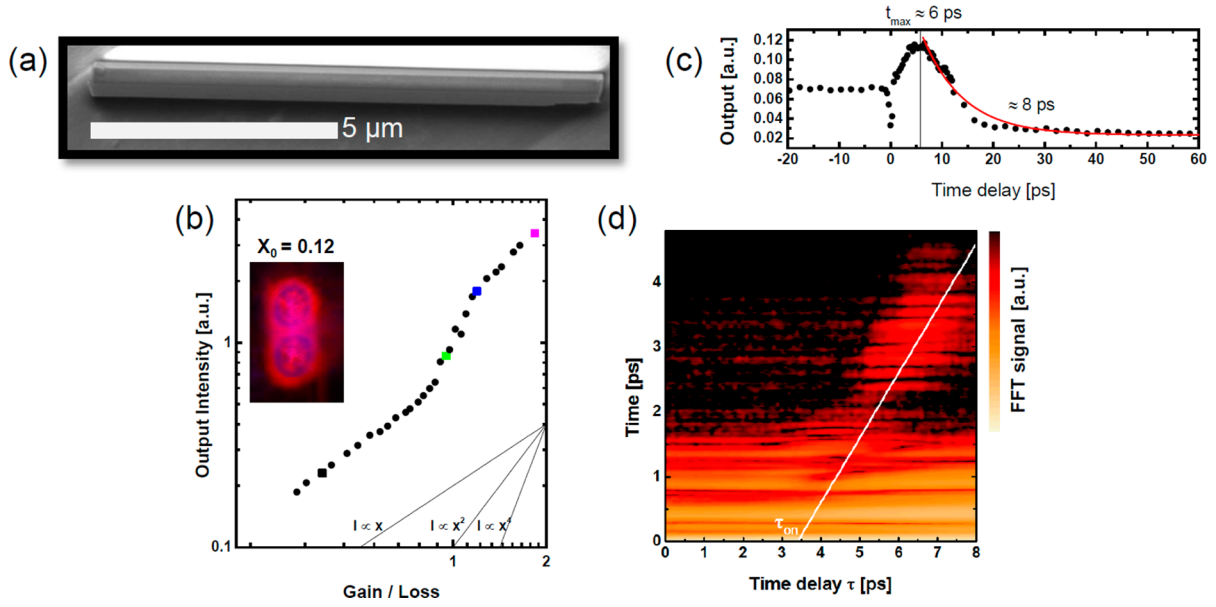

Figure 4. (a) SEM image of a GaN nanowire laser (length 10.5 μm, diameter ≈630−700 nm) lying on a 1.5 μm thick SiO_2 layer on Si substrate. (b) Power dependence of output intensity with a linear slope below threshold (gain/loss = 1) and superlinear increase around threshold indicating amplified spontaneous emission (ASE) followed by linear dependence indicating laser oscillations. The marked data points belong to the μPL spectra shown in Supporting Information Figure S5. The inset shows an optical image of the lasing GaN NW. (c) The total double-pump response of the GaN NW laser versus time delay τ for the strong Pump1 = 2 × I_{th} and the weak Pump2 = 0.2 × I_{th}. The measured data unambiguously follow the simulation from Figure 1c. (d) The Fourier transform of the double-pump response (in log scale) of the same GaN NW with a linear trend (white), whose x-axis intersect marks a value of τ_{on} = 3.4 ps.

where $\Delta\Phi$ is the spectral phase difference between both output pulses.[23] The modulation frequency therefore increases linearly as a function of τ_m. Indeed, in Figure 2a we observe the modulation of the spectral output of the nanowire laser, $\Delta I/I_0$, which also varies as a function of the time delay as suggested by eq 1. The modulation starts approximately between 2−3 ps and, as indicated by the line scans taken at 3.5 ps (green) and 4.5 ps (red), the modulation clearly increases in frequency with increasing time delay between the pump pulses. See also Supporting Information Figure S1. Subsequently, this spectral data was Fourier transformed into the time domain (Figure 2c), such that the spectral modulation becomes apparent as a sideband. The sideband follows a linear behavior attributed to the temporal delay between pump and output pulse: $\tau_{m=}\ \tau - (t_1 - t_2)$, which is schematically depicted also in Figure 1a,b. The decay of the sideband amplitude is associated with the resolving power of our spectrometer, which corresponds to a temporal delay of about 4 ps.[23] Because the laser system is still inverted or even close to inversion population when the weak Pump2 arrives, we reasonably assume that $t_1 \gg t_{2,}$ consistent with the simulated laser response.[23] Thus, the time $t_1 \approx \tau_{on}$, which is obtained as the x-axis intersect of the linear line, is the required time to establish an output pulse from an optically excited NW laser. For the given situation, we observe an onset time of $\tau_{on} \approx$ 2.5 ps for the ∼190 nm diameter CdS NW pumped at 355 nm. Other CdS NW lasers with different diameters reveal similar laser onset times of approximately 2.5 ps, indicating that this is a material dependent parameter, which is independent of the optical system and the laser mode(s). However, this value is more than twice that for ZnO NWs of $\tau_{on} \approx$ 1 ps under similar experimental conditions.[23] However, we note that the optical excitation energy of 3.49 eV (355 nm) is much closer to the bandgap of ZnO than it is to the bandgap of CdS; hence, a reduction in pump energy might draw a route to adjust the CdS laser onset time.

Therefore, the exact same CdS NW was subsequently measured using a reduced optical excitation energy of 2.95 eV corresponding to a wavelength of 420 nm. The lasing performance was again initially checked: Figure 3a compares the lasing output spectra obtained at twice the threshold using 420 nm (blue) and 355 nm (black) excitation. Both spectra nearly coincide as they reveal the identical longitudinal modes and similar overall intensities, although the gain envelope seems to be slightly shifted to higher emission energies. The output intensities as a function of the gain/loss ratio (inset of Figure 3a) coincide perfectly when fit to a multimode laser model.[26] Furthermore, the laser emission is independent of the pump wavelength predominantly polarized perpendicular to the NW axis (see Supporting Information Figure S2); thus, an impact of the excitation energy on the transverse lasing modes can be ruled out.

The case of a reduced pump energy is sketched in Figure 3b: referring to the semiconductor NWs as a multilevel laser system, the pump level (black horizontal line for 355 nm; blue for 420 nm) and the upper laser level represented by the quasi-Fermi levels for electron E_f^e and holes E_f^h (red horizontal line) get energetically closer. Thus, the states that the carriers have to thermalize through is significantly reduced leading to a faster onset time τ_{on}. Now, the double-pump approach is applied to exactly the same CdS NW as before (see Figure 2b) using the reduced pump energy at 420 nm measuring again the NW laser output temporally as well as spectrally. The visibility of the modulation frequency at a certain delay time τ is indeed higher for the 420 nm excitation as the laser onset time is decreased compared to 355 nm excitation (see Supporting Information Figure S3). The fast Fourier transform (FFT) signal shown in Figure 3c, which was obtained by the same evaluation as in

DOI: 10.1021/acs.nanolett.5b01271
Nano Lett. 2015, 15, 4637−4643

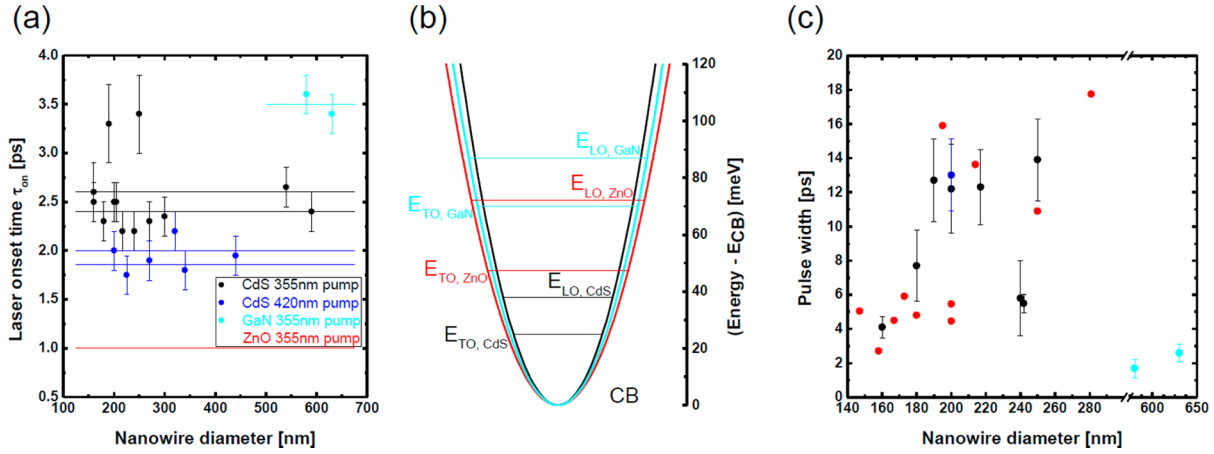

Figure 5. (a) Measured laser onset times τ_{on} versus nanowire diameter for GaN (cyan), CdS (black), and ZnO (red) pumped at 355 nm and CdS pumped at 420 nm (blue). The value for ZnO is taken from ref 23. The laser onset time is independent of the NW diameter as indicated by the horizontal lines. (b) Schematic drawing of the simplified parabolic conduction bands (CB) for CdS (black), ZnO (red), and GaN (cyan), where the different dispersions reflect the different effective electron masses. Additionally the energetic positions of the LO and TO phonons are marked as horizontal lines with the CB minimum chosen as zero. Below this marks the respective phonon may not contribute as energy loss channel for the charge carriers due to violation of energy conservation. (c) Laser output pulse width for CdS (black for 355 nm pump, blue for 420 nm pump), GaN (cyan), and ZnO (red) NW lasers versus the diameter. The data for ZnO NWs is again taken from ref 23.

Figure 2, also exhibits the signal sideband with a clear linear dependence. The intersection of this line with the *x*-axis is shifted to the lower value of $\tau_{on} \approx 2.0$ ps compared to the measurements shown in Figure 2. The approach to tune the pump energy is clearly capable of controlling the laser onset time of a single CdS NW laser.

The output P_{out} as a function of the time delay also closely coincides with the simulated response from Figure 1c (see Supporting Information Figure S4). We note that our measurement technique scans over relative short time delays (~80 ps) relative to the spontaneous recombination times in CdS (~1 ns).[27] In particular, we note a peak in the output power for a given time delay, t_{max}, which is attributed to absorption saturation in the nanowire following the first pump pulse. This is an indication of both the gain recovery time in the NW as well as the point at which the initial output pulse stops lasing.[23] Importantly, the t_{max} value for both pumping wavelengths matches at ~16−17 ps. The output pulse dynamics are therefore most likely unaffected by the change in pump energy, indicating the gain recovery time and pulse width to be a resonator morphology driven property of the NW laser, while the onset time is determined by the electronic properties of the semiconductor and the excitation wavelength. Note that the t_{max} value should most likely be affected by the decrease of τ_{on}, too. If the laser turns on more quickly, the lasing will occur faster and the t_{max} will be reached faster. However, since τ_{on} changes by just ~0.5 ps, it is too difficult to evaluate precisely whether t_{max} has changed.

Having determined the lasing dynamics of a single CdS NW laser, further insights are required in how the choice of the semiconductor material and different resonator properties influence the characteristic time values for τ_{on} and t_{max}. Therefore, photonic GaN NW lasers emitting in the UV spectral range were also investigated using the 355 nm excitation wavelength. Figure 4a shows the SEM image of an exemplary GaN NW (10.1 μm length, ~ 630−700 nm diameter) on SiO_2/Si substrate, on which the following lasing investigations were carried out. The evolution of the emission spectra with increasing pump power (see Supporting Information Figure S5) and the power dependence in Figure 4b prove lasing. The overall laser emission is predominantly polarized along the NW axis, but the single modes show partially also perpendicular polarized emission (see Supporting Information Figure S6). As indicated by the optical images (e.g., inset of Figure 4b) from the lasing GaN nanowires, the laser light is largely emitted from the end facets, thus the GaN NWs exhibit still FP-like cavity modes. Subsequently, the double-pump approach was utilized to explore the temporal dynamics of this GaN nanolaser. The output signal of the double-pump measurement in Figure 4c nicely depicts the expected course from the simulation with a well-pronounced $t_{max} \approx 6$ ps. The output pulse of the GaN NW terminates three times earlier than the pulse of the CdS NW investigated earlier. Furthermore, the decay rate for $\tau > t_{max}$ of ~8 ps is at least one order of magnitude faster than the respective value for ZnO NWs[23] and even more for CdS NWs. The evaluation of the FFT signal in Figure 4d leads to a laser onset time of ~3.4 ps. This value is surprisingly slow as the pumping energy is much closer to the bandgap compared to ZnO ($\tau_{on} \approx 1$ ps) and CdS NWs ($\tau_{on,\ 355\ nm} \approx 2.5$ ps; $\tau_{on,\ 420\ nm} \approx 2.0$ ps) but fits recent studies on the carrier dynamics in GaN nanorods.[28]

The onset time τ_{on} seems to be a material driven property of the nanolaser, while the output pulse width is largely determined by the resonator performance. In order to verify this assumption, we compare several NW devices made of the different semiconductor materials. Figure 5a shows the laser onset time for several different photonic NW lasers as a function of nanowire diameter. Adjusting the excitation wavelength to 355 nm results in the fastest laser onset for ZnO NWs of ~1 ps, followed by CdS NWs exhibiting a $\tau_{on} \approx$ 2.5 ps and GaN NWs having the slowest onset of ~3.5 ps, although the energy difference between excitation and emission is smallest for GaN. This indicates that the carrier relaxation in the semiconductor material, described by the energy loss rate (ELR), seems to be significantly different.

However, the concept of reducing the excitation energy to gain an accelerated τ_{on} is also proven in Figure 5a for CdS NWs; the procedure, which we applied for the CdS NW from

DOI: 10.1021/acs.nanolett.5b01271
Nano Lett. 2015, 15, 4637−4643

Figure 2b, was inverted for the CdS NW with a diameter of 270 nm. Yet, we measured at first at 420 nm excitation giving $\tau_{on,420\ nm} \approx 1.9$ ps, afterwards the pump was set to 355 nm leading to $\tau_{on,\ 355\ nm} \approx 2.3$ ps. Thus, we can conclude that the process can be reverted and adjusted freely. On average the onset time of CdS NWs decreases from $\tau_{on,355\ nm} = 2.50 \pm 0.10$ ps to $\tau_{on,420\ nm} = 1.93 \pm 0.07$ ps. Assuming that the reduced onset time only originates from the smaller number of electronic states, which the carriers have to scatter through during relaxation, we can convert this into an effective ELR of the whole carrier system of ~1 eV/ps. Pugnet et al. theoretically predicted the ELR in CdS to be ~1.9 eV/ps, assuming a lattice temperature of 4 K, a plasma (carrier) temperature of 500 K and a carrier density slightly above the Mott density.[29] Applying additionally the temperature dependence of the energy loss due to LO phonons,[30] we obtain an ELR for CdS at room temperature of ~1.1 eV/ps, which nicely agrees with our estimation. A further acceleration for CdS NW lasers toward $\tau_{on} \sim 1.6$ ps is expected for a pumping of 480 nm wavelength (see Supporting Information).

The different onset times for the various semiconductor materials arise from the processes following optical excitation, when carriers undergo microscopic many-body dynamics: spatial and temporal evolution with different characteristic times.[31] The initially created nonequilibrium (monochromatic distributed) carriers evolve toward equilibrium within femtosecond time scales via elastic and inelastic scattering as well as via carrier−carrier scattering.[32] However, the main contribution to the energy relaxation is provided via the emission of phonons,[33] thus we mainly need to consider the carrier−phonon interaction to explain the different onset times. Carrier diffusion is not considered here due to the low diffusion length within a few picoseconds.[34] Furthermore, we only consider electrons because (i) the photoexcited holes exhibit a much lower excess energy ΔE_h than the electrons ΔE_e, which is given by

$$\Delta E_{e(h)} = (E_{\hbar\omega} - E_g)\left(1 + \frac{m_{e(h)}}{m_{h(e)}}\right)^{-1} \quad (2)$$

where $E_{\hbar\omega}$ is the optical excitation energy, E_g is the bandgap energy, and $m_{e(h)}$ is the effective electron (hole) masses.[31] (ii) The hole relaxation rates in the three materials are higher due to their higher effective masses (see Table 1 in Supporting Information).[35,36,29] Figure 5b depicts the conduction band (CB) of CdS (black), GaN (cyan), and ZnO (red) with the respective energies for the longitudinal (LO) and transverse (TO) optical phonons. Electrons release their excess energy mainly by successive emission of LO phonons and relax toward the CB minimum,[32] until the electrons do not possess enough energy and the LO phonon emission is forbidden by energy conservation.[37] The electron−LO phonon interaction reveals the highest ELR among the electron−phonon interactions and is described by the long-range Fröhlich interaction. The Fröhlich coupling constant α can be calculated according to ref 38 and is the highest for ZnO and the lowest for GaN (see Table 1 in Supporting Information). The ELR due to emission of LO phonons is directly proportional to α. The electron relaxation in GaN suffers furthermore from the hot phonon effect reducing the theoretical LO emission rate as well as the ELR by a factor of ~20.[30,32,37] Electrons with a remaining excess energy between LO and TO phonon mainly relax by the short-range interaction with TO phonons described by the optical deformation potential.[29] The respective TO−ELR range is at least one order of magnitude lower than the LO−ELR.[32,29] Electrons, which reach an energy below the TO energy, only interact further with acoustic phonons. The electron-acoustic phonon interactions are described by the acoustic deformation potential and the piezoacoustical interaction potential.[39,29] Comparing the respective quantities, as shown in the Supporting Information, we can qualitatively explain the differences in relaxation times for CdS, GaN, and ZnO. The carrier relaxation in GaN is slower for two main reasons: the hot phonon effect significantly limits the electron−LO phonon interaction; thus, the respective ELR is at least ~5 (30) times smaller than the ELR of CdS (ZnO) at the same carrier temperature.[37] However, the carrier temperature can be expected to be even higher in CdS and ZnO, because the optical excitation energy relative to the bandgap energy is larger here.[40] Thus, the ELR in CdS and ZnO is even more increased. The rather high LO and TO phonon energies compared especially to CdS cause a large energetic region, which the carriers have to scatter through by the rather weak interaction with TO and acoustical phonons. The technological relevant GaAs NW lasers[18] exhibit also a weak electron−phonon coupling and should also suffer significantly from the hot phonon effect.[31,37] We therefore predict an even slower onset-time for GaAs NW lasers.

We determined the pulse width as $\tau_{pulse} = t_{max} - \tau_{on}$ for several NW lasers as a function of diameter shown in Figure 5c. The pulse widths of photonic ZnO NWs were already discussed in detail in.[23] ZnO nanolasers reveal output pulse widths between 5−15 ps with longer pulses occurring for thicker wires. Furthermore, the abrupt pulse width increase for ZnO NW laser resonators near 200 nm diameter from 5 to 15 ps is accompanied by a change in laser emission polarization from a polarization along the NW to perpendicular polarized emission.[23] Note, τ_{on} does not show any dependence on the NW diameter. We observed a similar trend for CdS NW lasers except for the three thickest wires. This behavior is likely caused by a switching from single transverse (HE_{11}) mode lasing toward high order (TE_{01}) mode lasing in thicker wires. The abrupt increase in pulse width for the CdS NW lasers occurs at a diameter of ~180 nm, which fits with our interpretation of this transition.[20] Note that the three thickest CdS NWs exhibit diameters providing efficient mode confinement even to additional higher order modes (such as HE_{21}, TM_{01}).[20] The expected multi high order mode lasing or mode competition can drastically affect the output pulse width. The same explanation also seems to fit for the rather thick GaN NW laser, which reveal a significantly shorter pulse width of ~2−3 ps, which is likely caused by multiple transverse modes competing for gain, as indicated by their spectra (see Supporting Information Figure S5).

In conclusion, the ultrafast laser dynamics of semiconductor photonic NW lasers, laser onset time, gain recovery time, and pulse width, were accessed by applying a double-pump measurement. Since the onset time τ_{on} is a material dynamics driven parameter of the semiconductor, the microscopic carrier−phonon interaction strength is considered to cause the different values for GaN, ZnO, and CdS. Among the so far investigated semiconductor NW lasers, ZnO reveals the fastest onset time due to the strongest carrier−phonon coupling. Other semiconductor NW lasers (ZnS, ZnSe, CdSe, InGaN, GaAs) are also expected to be slower, because they suffer from weaker carrier−phonon coupling, slowing down the carrier

DOI: 10.1021/acs.nanolett.5b01271
Nano Lett. 2015, 15, 4637−4643

relaxation.[41,42,29] However, the adjustment of the excitation energy provides an efficient way to tune the onset time for a particular semiconductor material. In contrast, the output pulse width is largely influenced by photonics: the NW resonator and the transverse photonic modes propagating within. However, a further acceleration of the ultrafast nanolasing requires a proper choice of gain material with faster carrier relaxation as well as an optical system going beyond photonics, as we obtain the shortest pulse width from the fundamental photonic mode.

■ ASSOCIATED CONTENT

Supporting Information

Sample preparation, optical setup, and additional figures. The Supporting Information is available free of charge on the ACS Publications website at DOI: 10.1021/acs.nanolett.5b01271.

■ AUTHOR INFORMATION

Corresponding Authors

*E-mail: robert.roeder@uni-jena.de.
*E-mail: carsten.ronning@uni-jena.de.

Author Contributions

The nanowires were grown by R.R. and C.T., the experimental measurements were conducted by R.R. and T.P.H.S.; results were discussed and interpreted by all authors; the manuscript was written by R.R. with feedback from all authors. All authors have given approval to the final version of the manuscript. The authors declare no competing financial interest.

Notes

The authors declare no competing financial interest.

■ ACKNOWLEDGMENTS

The authors gratefully acknowledge funding by the German Research Society (DFG) within the project FOR1616.

■ REFERENCES

(1) Stockman, M. *Nat. Phys.* **2014**, *10*, 799−800.
(2) Lu, Y.-J.; Kim, J.; Chen, H.-Y.; Wu, C.; Dabidian, N.; Sanders, C. E.; Wang, C.-Y.; Lu, M.-Y.; Li, B.-H.; Qiu, X.; Chang, W.-H.; Chen, L.-J.; Shvets, G.; Shih, C.-K.; Gwo, S. *Science* **2012**, *337*, 450−453.
(3) Anker, J. N.; Hall, W. P.; Lyandres, O.; Shah, N. C.; Zhao, J.; Van Duyne, R. P. *Nat. Mater.* **2008**, *7*, 442−453.
(4) Sirbuly, D. J.; Law, M.; Pauzauskie, P.; Yan, H.; Maslov, A. V.; Knutsen, K.; Ning, C.-Z.; Saykally, R. J.; Yang, P. *Proc. Natl. Acad. Sci. U.S.A.* **2005**, *102*, 7800−7805.
(5) Yan, R.; Gargas, D.; Yang, P. *Nat. Photonics* **2009**, *3*, 569−576.
(6) Voss, T.; Kudyk, I.; Wischmeier, L.; Gutowski, J. *Phys. Status Solidi B* **2009**, *246*, 311−314.
(7) Yu, H.; Fang, W.; Wu, X.; Lin, X.; Tong, L.; Liu, W.; Wang, A.; Shen, Y. R. *Nano Lett.* **2014**, *14*, 3487−3490.
(8) Piccione, B.; Cho, C.-H.; van Vugt, L. K.; Agarwal, R. *Nat. Nanotechnol.* **2012**, *7*, 640−645.
(9) Bohnert, K.; Schmieder, G.; El-Dessouki, S.; Klingshirn, C. *Solid State Commun.* **1978**, *27*, 295−299.
(10) Klingshirn, C.; Fallert, J.; Zhou, H.; Sartor, J.; Thiele, C.; Maier-Flaig, F.; Schneider, D.; Kalt, H. *Phys. Status Solidi B* **2010**, *247*, 1424−1447.
(11) Voss, T.; Svacha, G.; Mazur, E.; Müller, S.; Ronning, C.; Konjhodzic, D.; Marlow, F. *Nano Lett.* **2007**, *7*, 3675−3680.
(12) Zimmler, M.; Bao, J.; Capasso, F.; Müller, S.; Ronning, C. *Appl. Phys. Lett.* **2008**, *93*, 051101.
(13) Johnson, J. C.; Choi, H.-J.; Knutsen, K. P.; Schaller, R. D.; Yang, P.; Saykally, R. J. *Nat. Mater.* **2002**, *1*, 106−110.
(14) Röder, R.; Wille, M.; Geburt, S.; Rensberg, J.; Zhang, M.; Lu, J. G.; Capasso, F.; Buschlinger, R.; Peschel, U.; Ronning, C. *Nano Lett.* **2013**, *13*, 3602−3606.
(15) Qian, F.; Li, Y.; Gradecak, S.; Park, H.-G.; Dong, Y.; Ding, Y.; Wang, Z. L.; Lieber, C. M. *Nat. Mater.* **2008**, *7*, 701−706.
(16) Zimmler, M.; Capasso, F.; Müller, S.; Ronning, C. *Semicond. Sci. Technol.* **2010**, *25*, 024001.
(17) Geburt, S.; Thielmann, A.; Röder, R.; Borschel, C.; McDonnell, A.; Kozlik, M.; Kühnel, J.; Sunter, K. A.; Capasso, F.; Ronning, C. *Nanotechnology* **2012**, *23*, 365204.
(18) Saxena, D.; Mokkapati, S.; Parkinson, P.; Jiang, N.; Gao, Q.; Tan, H. H.; Jagadish, C. *Nat. Photonics* **2013**, *7*, 963−968.
(19) Hurtado, A.; Xu, H.; Wright, J. B.; Liu, S.; Li, Q.; Wang, G. T.; Luk, T. S.; Figiel, J. J.; Cross, K.; Balakrishnan, G.; Lester, L. F.; Brener, I. *Appl. Phys. Lett.* **2013**, *103*, 251107.
(20) Röder, R.; Ploss, D.; Kriesch, A.; Buschlinger, R.; Geburt, S.; Peschel, U.; Ronning, C. *J. Phys. D: Appl. Phys.* **2014**, *47*, 394012.
(21) Gao, H.; Fu, A.; Andrews, S. C.; Yang, P. *Proc. Natl. Acad. Sci. U.S.A.* **2013**, *110*, 865−869.
(22) Xiao, Y.; Meng, C.; Wang, P.; Ye, Y.; Yu, H.; Wang, S.; Gu, F.; Dai, L.; Tong, L. *Nano Lett.* **2011**, *11*, 1122−1126.
(23) Sidiropoulos, T. P. H.; Röder, R.; Geburt, S.; Hess, O.; Maier, S. A.; Ronning, C.; Oulton, R. F. *Nat. Phys.* **2014**, *10*, 870−876.
(24) Tessarek, C.; Röder, R.; Michalsky, T.; Geburt, S.; Franke, H.; Schmidt-Grund, R.; Heilmann, M.; Hoffmann, B.; Ronning, C.; Grundmann, M.; Christiansen, S. *ACS Photonics* **2014**, *1*, 990−997.
(25) Maslov, A.; Ning, C. *Appl. Phys. Lett.* **2003**, *83*, 1237.
(26) Casperson, L. *J. Appl. Phys.* **1975**, *46*, 5194−5201.
(27) Wiesner, P.; Heim, U. *Phys. Rev. B* **1975**, *11*, 3071−3077.
(28) Yang, C.-Y.; Chia, C.-T.; Chen, H.-Y.; Gwo, S.; Lin, K.-H. *Appl. Phys. Lett.* **2014**, *105*, 212105.
(29) Pugnet, M.; Collet, J.; Cornet, A. *Solid State Commun.* **1981**, *38*, 531−536.
(30) Ye, H.; Wicks, G. W.; Fauchet, P. M. *Appl. Phys. Lett.* **1999**, *74*, 711−713.
(31) Shah, J. *Solid-State Electron.* **1978**, *21*, 43−50.
(32) Zhang, X. B.; Taliercio, T.; Kolliakos, S.; Lefebvre, P. *J. Phys.: Condens. Matter* **2001**, *13*, 7053.
(33) Othonos, A. *J. Appl. Phys.* **1998**, *83*, 1789−1830.
(34) Saito, H.; Göbel, E. O. *Phys. Rev. B* **1985**, *31*, 2360−2369.
(35) Prabhu, S. S.; Vengurlekar, A. S. *J. Appl. Phys.* **2004**, *95*, 7803−7812.
(36) Zukauskas, A.; Tamulaitis, G.; Gaska, R.; Shur, M.; Khan, M.; Yang, J. *Phys. Status Solidi B* **1999**, *216*, 495−499.
(37) Shah, J. *Hot Carriers in Semiconductor Nanostructures: Physics and Applications*; Elsevier: New York, 2012.
(38) Fröhlich, H. *Adv. Phys.* **1954**, *3*, 325−361.
(39) Yu, P. Y.; Cardona, M. *Fundamentals of Semiconductors*; Springer: New York, 2005.
(40) Wang, Y.; Jackson, H. E.; Smith, L. M.; Burgess, T.; Paiman, S.; Gao, Q.; Tan, H. H.; Jagadish, C. *Nano Lett.* **2014**, *14*, 7153−7160.
(41) Yang, X.; Xu, C.; Giles, N. C. *J. Appl. Phys.* **2008**, *104*, 073727.
(42) Prabhu, S. S.; Vengurlekar, A. S.; Roy, S. K.; Shah, J. *Phys. Rev. B* **1995**, *51*, 14233−14246.

DOI: 10.1021/acs.nanolett.5b01271
Nano Lett. 2015, 15, 4637−4643